Hybrid Electric Vehicle Power Management Solutions Based on Isolated and Nonisolated Configurations of Multilevel Modular Capacitor-Clamped Converter

Faisal H. Khan, *Member, IEEE*, Leon M. Tolbert, *Senior Member, IEEE*, and William E. Webb, *Member, IEEE*

Abstract—**This paper presents the various configurations of a multilevel modular capacitor-clamped converter (MMCCC), and it reveals many useful and new formations of the original MMCCC for transferring power in either an isolated or nonisolated manner. The various features of the original MMCCC circuit are best suited for a multibus system in future plug-in hybrid or fuel-cell-powered vehicles' drive train. The original MMCCC is capable of bidirectional power transfer using multilevel modular structure with capacitor-clamped topology. It has a nonisolated structure, and it offers very high efficiency even at partial loads. This circuit was modified to integrate single or multiple high-frequency transformers by using the intermediate voltage nodes of the converter. On the other hand, a special formation of the MMCCC can exhibit dc outputs offering limited isolation without using any isolation transformer. This modified version can produce a high conversion ratio from a limited number of components and has several useful applications in providing power to multiple low-voltage loads in a hybrid or electric automobile. This paper will investigate the origin of generating ac outputs from the MMCCC and shows how the transformer-free version can be modified to create limited isolation from the circuit. In addition, this paper will compare various modified forms of the MMCCC topology with existing dc–dc converter circuits from compactness and component utilization perspectives.**

Index Terms—**Fuel-cell vehicle, isolated dc–dc converter, multilevel dc–dc converter, multilevel modular capacitor-clamped converter (MMCCC), plug-in hybrid vehicle.**

I. Introduction

CAPACITOR-clamped dc–dc converters have features that are advantageous over other topologies of dc–dc converters based on the inductive energy transfer method (IETM) such as buck, boost, and buck–boost converters. The key advantage of the capacitive energy transfer method is the high-efficiency operation that is an inherent nature of many capacitor-clamped or switched-capacitor circuits. However, one of the favorable features of the well-known IETM converters is

the scope of achieving isolated dc outputs using high-frequency transformers. This isolation is found essential when the converter needs to be integrated between low-voltage (LV) and high-voltage (HV) buses [1]–[5], and the present trend indicates that this multivoltage bus architecture will be very common in plug-in hybrid or future fuel-cell automobiles [1], [3]. A dc–dc converter suitable for this application still belongs to an IETM converter family in most cases. In spite of having many advantageous attributes, capacitor-clamped converters were rarely investigated to achieve ac outputs to obtain a sustainable solution for several applications that require high-efficiency operation and modular configuration.

Bidirectional power management is an important attribute of a dc–dc converter used in several automotive applications such as hybrid electric or plug-in hybrid electric vehicles' propulsion system. In a hybrid electric vehicle, many electrical loads may exist, which are grouped into two main categories, depending on the voltages they use. Fig. 1 shows the typical arrangement of the power electronic modules in a fuel-cell-powered vehicle [3]. The main traction motor is powered from the HV bus (around 500 V). The fuel cell may directly power the inverter or an intermediate unidirectional dc–dc boost converter may be used. There are also LV loads that need to be powered from a LV source in the range of 40–50 V. This LV source could be a battery or a stepped down voltage from the HV battery pack or any other source. When the HV source is a fuel cell, the LV source is normally a battery pack that propels the vehicle during start-up and provides ancillary services to power up the fuel-cell system [3]. The dc–dc converter works in the up-conversion mode and has to deliver the full power required by the inverter. Once the fuel cell is operational, it provides power to the main motor and LV loads and charges the battery using the dc–dc converter in buck mode. Thus, a dc–dc converter used in the system must have the capability to deliver power in both directions, depending on the state of the fuel cell or the battery voltage. In addition to the power flow architecture shown in Fig. 1, there exist many other power management strategies described in [3]. Thus, the rating of the dc–dc converter is manufacturer specific and can range from several kilowatts to as high as 100 kW.

A capacitor-clamped converter [6]–[8] usually has more transistors for a certain conversion ratio (CR) compared to the classical IETM dc–dc converters [9]–[16] commonly used in
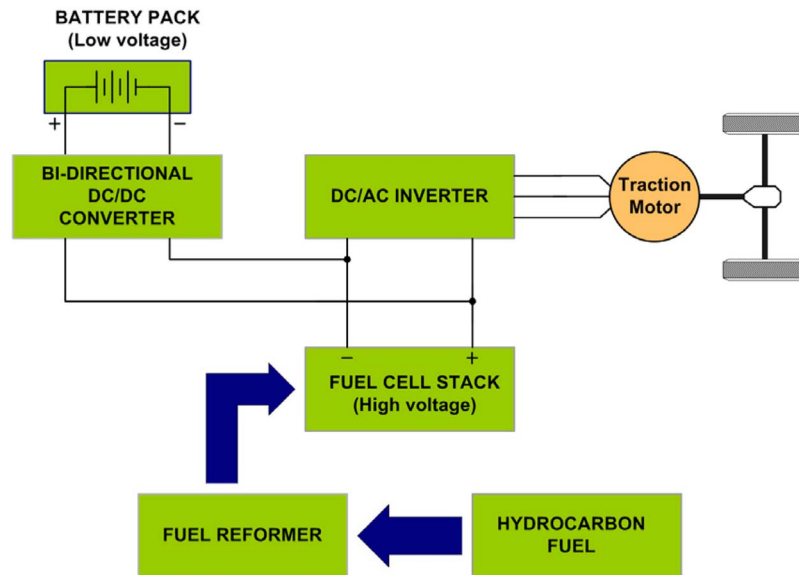
Fig. 1.   Typical topological arrangement of a hybrid fuel-cell vehicle drive train [3].

automotive applications. Therefore, the key difference between a multilevel converter and other genres of dc–dc converters is the distributed stress across the switching elements in the circuit. Thus, the total power handling capability is contributed by multiple transistors and capacitors used in a capacitor-clamped or any other multilevel dc–dc converter circuit. This property of capacitor-clamped converters is advantageous over IETM converters such as buck or boost, where the entire voltage stress is experienced by a single transistor. The capacitor-clamped topologies are usually nonisolated, and they produce CR of integer values. In addition, the number of voltage levels present in those circuits has a linear relationship with the CR of the circuit. The well-known flying capacitor multilevel dc–dc converter (FCMDC) [17] has a CR that is equal to $(N - 1)$, where N is the number of voltage levels present in the circuit. In the multilevel modular capacitor-clamped converter (MM-CCC), the number of voltage levels is equal to the CR of the circuit [17]. Thus, it requires many transistors to form these voltage levels when the circuit has to produce a high CR. This is why capacitor-clamped converters may lose their importance and usefulness in many applications where high CR is needed and less component count is a prime factor.

The use of a higher number of transistors in a converter circuit can be justified if some capacitor-clamped converters are comparable with the interleaved design of conventional IETM converters. In interleaved buck or boost converters, multiple current paths are connected in parallel to reduce the current stress for a single switch [16]. On the other hand, capacitor-clamped converters such as FCMDC [17] offer the stacked-capacitor scheme (multiple capacitors connected in series), and MMCCC offers both stacked-capacitor and cascade configurations to reduce the voltage stress across one single transistor. In addition, the MMCCC circuit can also reduce the current stress by cascading and paralleling current paths inside the circuit [17].

The MMCCC construction is based on capacitor-clamped topology. However, the circuit uses a higher number of tran-

sistors compared to the FCMDC circuit to offer current path paralleling and modularity in the circuit. For a CR equal to N, the FCMDC circuit requires $2N$ number of transistors, and the MMCCC requires $(3N - 2)$ number of transistors. It was shown in [18] how the MMCCC has a better component utilization (CU) compared to the FCMDC converter, although the MMCCC requires more transistors for any CR. In continuation of the improvement phases of the MMCCC, a modified version of the MMCCC circuit will be presented in this paper, which can offer very high CR without having large number of transistors. In addition, this paper will also present various configurations of the isolated form of the MMCCC circuit.

II. NEED FOR ISOLATION

In future hybrid electric or fuel-cell automobiles, a bidirectional dc–dc converter is an integral part of the multivoltage dc architecture. This dc–dc converter maintains a power balance between the fuel cell and any energy storage inside the vehicle and provides continuous power to the drive train [3]. A new topology of multilevel dc–dc converter was shown in [18], which maintains a power balance between 250- and 42-V systems. However, there are still 12-V (or 14-V) electrical loads in the vehicle, and another isolated dc–dc converter is required to establish an energy balance between the 42- and 14-V buses. Because many consumer appliances may be connected to the 14-V bus, it should be electrically isolated from the HV bus [12]. A solution to this problem would be using a second dc–dc converter that builds the power flow path between the 42- and 14-V buses and creates necessary isolation. However, the use of two dc–dc converters involves substantial cost and complexity in the system, and it may not be possible to achieve a compact form factor for automobile applications. In this paper, the proposed converter could possibly eliminate the need for the second stage and combines the two dc–dc conversion steps. Thereby, it is possible to generate isolated 14-V output from the new design without sacrificing various advantageous features of
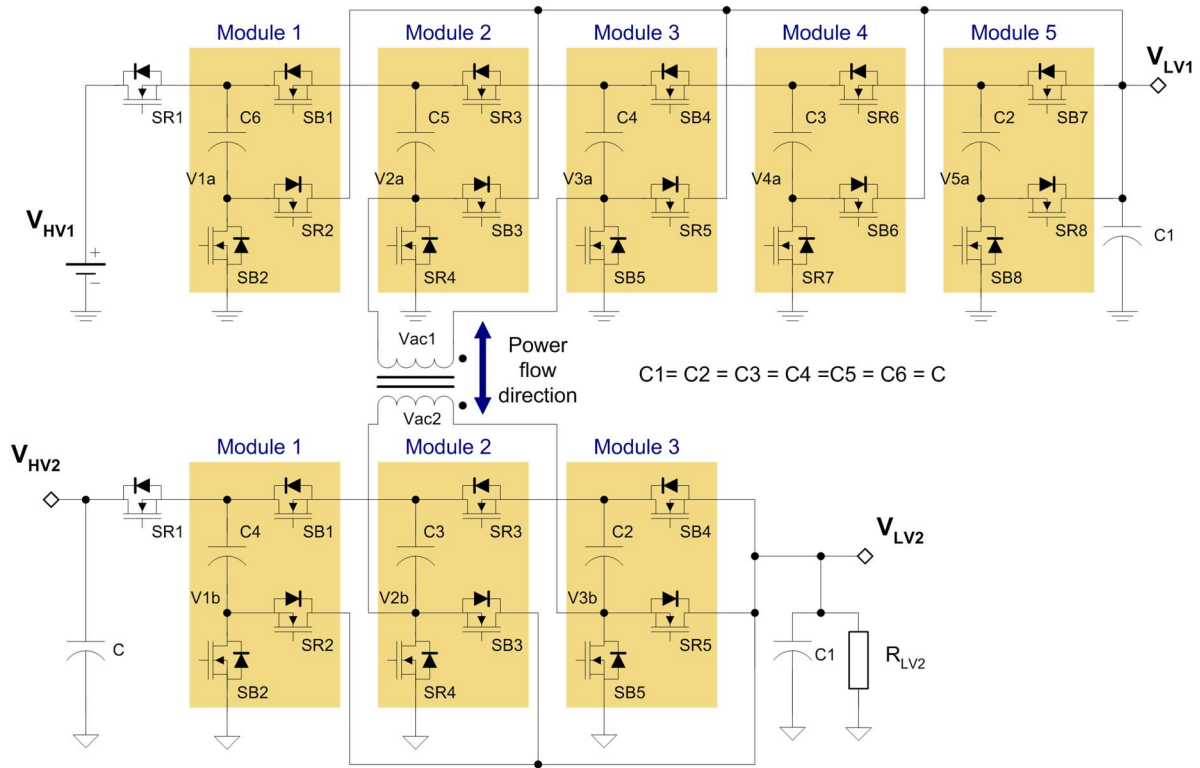
Fig. 2. Schematic of the isolated MMCCC constructed from two nonisolated MMCCCs.

the MMCCC. Several other examples and importance of having isolated outputs in a dc–dc converter were found in [12] and [19]. This paper presents the proof of concept prototypes of both isolated and universal MMCCCs that can be scaled up to as high as 100 kW or more.

III. ISOLATED MMCCC

The concept of integrating multiple sources in a dc–dc converter for hybrid electric vehicles was found in several literatures [19]–[24]. In this continuation, the unique multiple load and source integration capability was one of the strengths of the MMCCC circuit presented in [25]. It was shown in [26] how the MMCCC can generate high-frequency ac outputs using its modular structure. This feature of the MMCCC can be used to combine two MMCCC circuits with a transformer to provide coupling between the two circuits. In Fig. 2, circuit 1 shown on top is a six-level MMCCC establishing the energy balance between the 250- and 42-V buses. Circuit 2 shown at the bottom is a four-level MMCCC circuit that has three modules. For proper operation, various subintervals in the switching operation of both circuits should be synchronized, and this includes the use of a common clock circuit to drive both MMCCC blocks in a synchronized way.

The various advantages of the isolated version of the MMCCC are not limited to the circuit shown in Fig. 2. Rather, there are many other ways to generate isolated dc outputs from the original MMCCC. Fig. 3(a) shows another approach where the MMCCC is coupled to an H-bridge stage to create an isolated bidirectional dc port. This bridge circuit could adopt pulsewidth modulation, and various CRs including fractional

values can be generated from the hybrid architecture. Fig. 3(b) shows a simpler solution where the isolated ac outputs are rectified to dc voltage by simply adding a passive rectifier stage. This version offers only unidirectional power transfer operation.

Fig. 4 shows the practical implementation of the topology shown in Fig. 3(a), and this circuit uses a center-tapped transformer where the circuit adopts a special transformer winding and can take advantage of the various ac nodes available in the MMCCC circuit [26]. The secondary side is constructed from a standard H-bridge to obtain the bidirectional power transfer ability.

The isolated version of MMCCC shown in Fig. 2 has many advantages over the three configurations shown in Figs. 3 and 4. In Fig. 2, the circuit constructs a power management system among various sources and loads by virtue of the MMCCC's multiload/source feature [25]. Thus, it is possible to connect multiple voltage sources and loads at various nodes of the six- and four-level MMCCC sides. The topology shown in Fig. 3(a) allows the integration of only one source and one load at the H-bridge side of the converter, although multiple sources could still be integrated on the MMCCC side. The configuration shown in Fig. 3(b) allows one way power transfer from the MMCCC side to the passive rectifier side. However, this circuit should offer lower cost and moderate efficiency compared to the circuits shown in Figs. 2–4.

IV. CIRCUIT CONSTRUCTION AND OPERATION

Although the MMCCC circuit is a dc–dc converter, it can also produce ac outputs having frequency that is equal to the
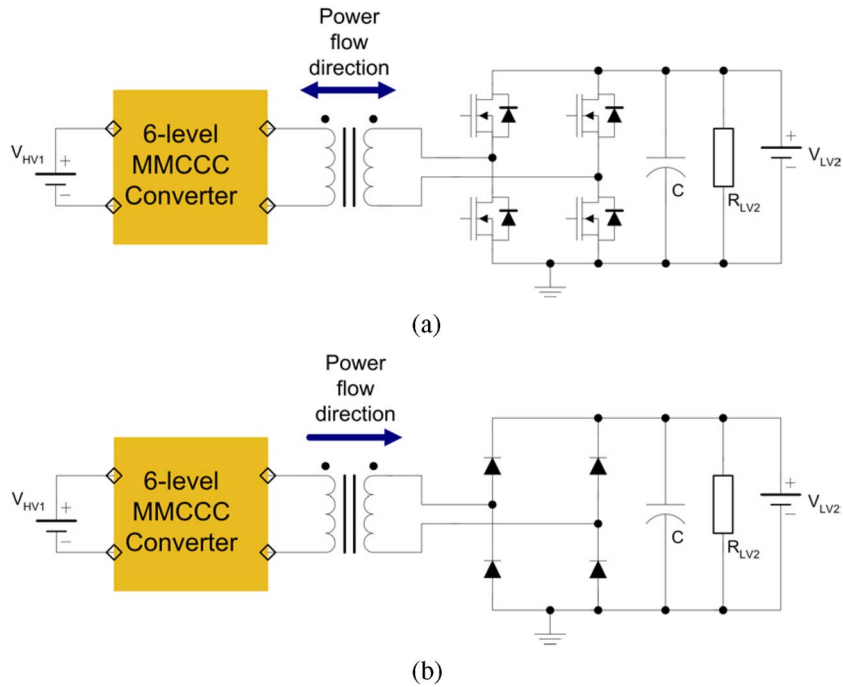
Fig. 3.   Isolated versions of the MMCCC with (a) H-bridge secondary side and (b) secondary side with a passive rectifier.
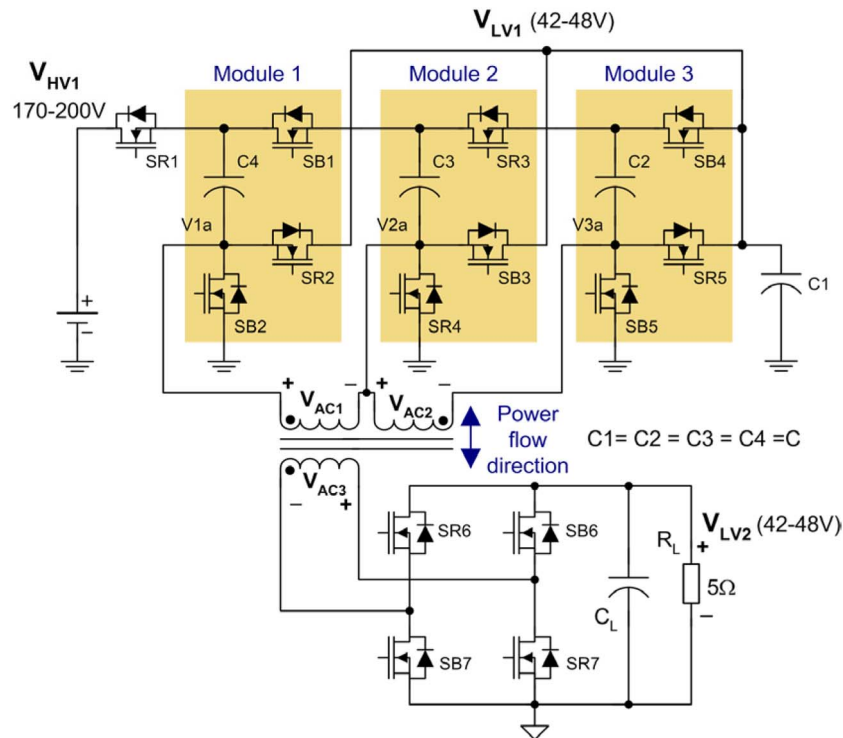

Fig. 4.   Isolated version of a four-level MMCCC with center-tap transformer.

switching frequency of the converter. It was shown in [26] how the MMCCC can generate ac outputs with amplitude close to one $V_{\rm LV}$ between two ac nodes in the MMCCC, and this amplitude is independent of the CR of the circuit. Thus, if a transformer of turn ratio $1:1$ is connected across the ac terminals of the MMCCC circuit and another MMCCC circuit is connected at the other terminals of the transformer, this

pair of MMCCC circuits forms a bidirectional architecture that allows the integration of loads in isolated and nonisolated manners. In Fig. 2, when a 252-V source is connected at $V_{\rm HV1}$, it is possible to produce a nonisolated 42-V output at $V_{\rm LV1}$, an isolated voltage of amplitude 42 V at $V_{\rm LV2}$, and an isolated 168-V output at $V_{\rm HV2}$ at no-load condition. In the same way, if a 168-V source is connected at $V_{\rm HV2}$, it is possible to achieve
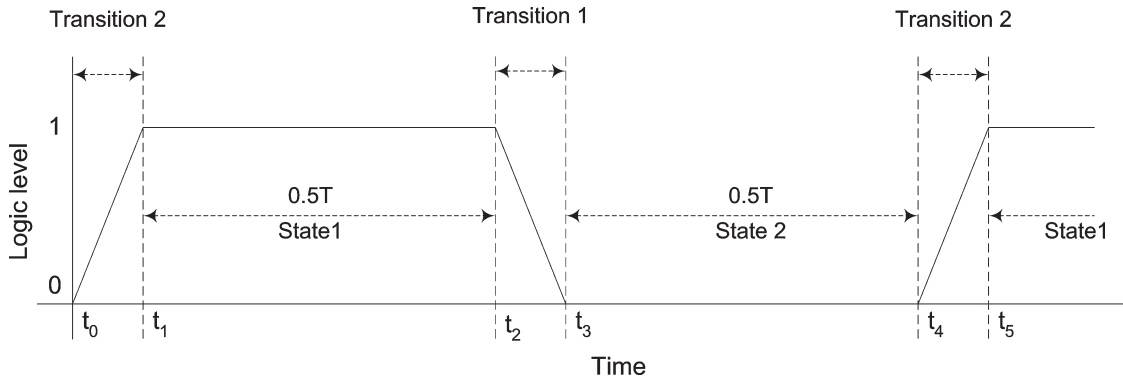
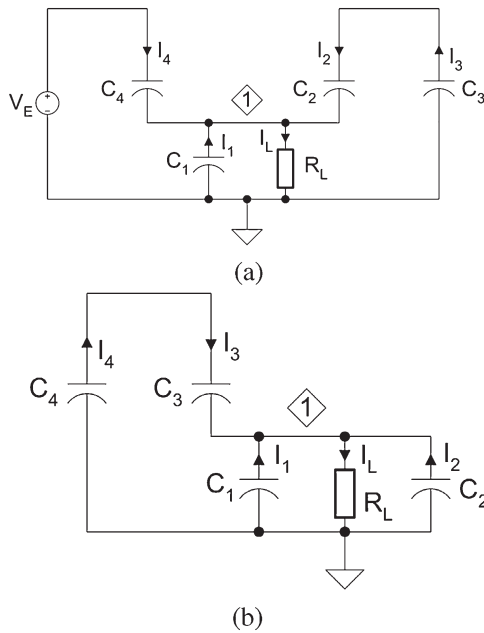Fig. 5. Timing diagram of the switching states of a four-level MMCCC.

Fig. 6. Equivalent circuits of a four-level MMCCC circuit at two subintervals. (a) During subinterval 1. (b) During subinterval 2.

a nonisolated 42-V output at V_{LV2}, an isolated 42-V output at V_{LV1}, and an isolated 252-V output at node V_{HV1} at no-load condition. By changing the transformer turn ratio to 3 : 1, an isolated 14-V output can be achieved at V_{LV2} and a nonisolated 42-V output can achieved at V_{LV1} node with a 252-V source connected at V_{HV1}.

The MMCCC circuit has two switching state subintervals, and in each subinterval, approximately one half of the transistors are ON. The timing diagram of the MMCCC circuit is shown in Fig. 5, and the corresponding equivalent circuit diagram for a four-level MMCCC is shown in Fig. 6. For the simplicity of the analysis, it is assumed that power is flowing from the four-level MMCCC to the six-level converter side in Fig. 2. During state 1 in the four-level MMCCC circuit (shown in Fig. 2), all the SRx ($SR_1, SR_2, \dots$) transistors are ON, and all the SB$_X$ ($SB_1, SB_2, \dots$) transistors are OFF. Thus, the voltage at V_{2b} is zero, and the voltage at V_{3b} is V_{LV2} during this interval. In the same way, the voltage at node V_{2b} is V_{LV2}, and it is zero at node V_{3b} during the second subinterval. Thus, the voltage difference across V_{2b} and V_{3b} is $\pm V_{LV2}$ or $\pm V_{C1}$.

If the expression of the voltage V_{C1} is found for these two subintervals, it is possible to determine the voltage across the transformer at steady-state condition.

When a transformer is used in a dc–dc converter circuit, the volt–second balance inside the transformer must be confirmed to ensure no residual flux buildup inside the transformer [27]. In an H-bridge circuit, this balance is done by clamping the voltage of the primary winding to the input dc voltage in both subintervals. The volt–second areas in positive and negative half cycles are balanced by clamping the voltage to ± 1 V_{LV} in the MMCCC.

V. ISOLATED MMCCC: SIMULATION RESULTS

To verify the concept of the new configuration, the schematic shown in Fig. 4 was simulated in PSIM to generate the voltages at V_{LV1} and V_{LV2} for no-load and at 5-Ω loading conditions, as well as voltages V_{AC1}, V_{AC2}, and V_{AC3}. A PSIM model of the actual transformer used in the experiment was used to generate these results. Used inside the MMCCC were 4500-μF capacitors with low equivalent series resistance (ESR), and a 1500-μF capacitor was used as C_L. A 5-Ω resistive load was used as R_L. The actual values of the R_{DS} of the MOSFETs used in the prototype (IXFR120N20) were used in the simulation, and this value was 0.017 Ω. The transformer turn ratio was 1 : 1.

The simulation results were generated by operating the MMCCC circuit in a down-conversion mode, and a 156-V source was connected as V_{HV1} so that the input power is 300 W. Fig. 7(a) shows the no-load voltages at V_{LV1} and V_{LV2}, and both of them were exactly one fourth of the input voltage because there was no voltage drop across the current path at zero current level. When the isolated LV side node was loaded with a 5-Ω load, it went down to 38.11 V, and V_{LV1} went to 38.68 V. These small voltage variations at these terminals took place due to the voltage drop across the MOSFET R_{DS}, capacitor ESR, and the transformer windings. The simulation results for V_{LV1} and V_{LV2} are shown in Fig. 7(b).

Fig. 8(a) shows the no-load voltages generated across the primary-side windings of the transformer (V_{AC1} and V_{AC2}), and Fig. 8(b) shows these voltages at full load (400 W). The voltages across the transformer had a small negative slope that indicates the decaying voltage across the clamp capacitors inside the MMCCC.
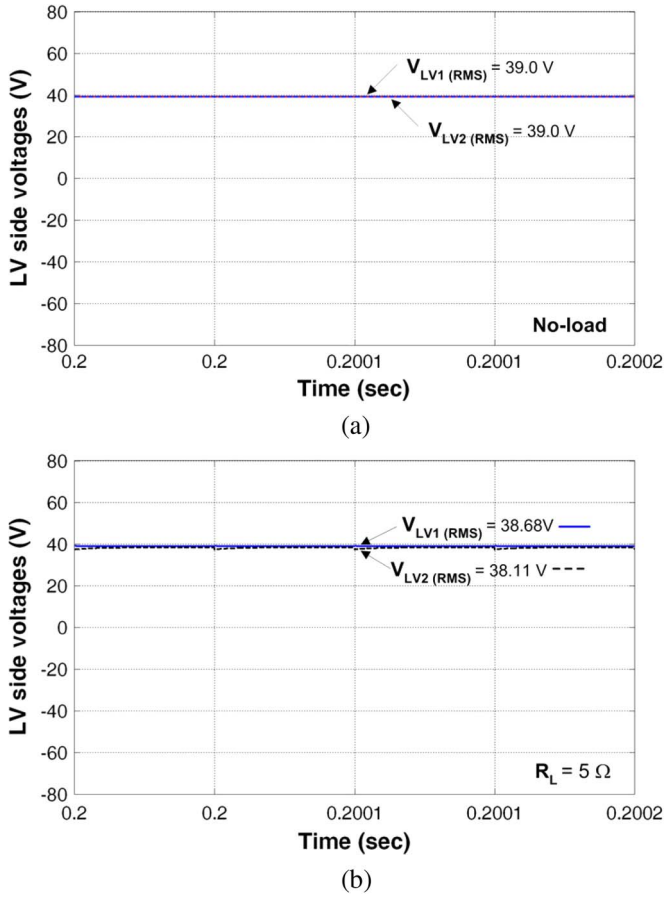
(a)

(b)

Fig. 7.   Simulation results of the isolated MMCCC circuit in the down-conversion mode. (a) DC output voltages at no-load condition. (b) Voltages with 5-Ω load connected at LV2 node. For both simulations, $V_{\mathrm{HV1}} = 156$ V.

(a)

(b)

Fig. 8.   Simulation results of the primary-side ac voltages of the transformer in Fig. 4. (a) At no-load condition. (b) With a 5-Ω load connected to the LV2 node. For both simulations, $V_{\mathrm{HV1}} = 179.75$ V.

VI. ISOLATED MMCCC: EXPERIMENTAL RESULTS

A 400-W four-level MMCCC was modified to achieve isolated dc outputs. This converter was designed to be used with the future 42-V Powernet, thus enabling the converter's LV side to connect to a 42-V source or load. The HV side voltage could be in the range of 170–200 V. A ferrite core transformer with 20 turns in each primary winding and 20 turns in the secondary winding was constructed to be used in the configuration shown in Fig. 4. The values of the various components were consistent with the simulation setup. The experimental setup is shown in Fig. 9. Figs. 10–14 show the various experimental results obtained from this 400-W prototype.

Fig. 10(a) and (b) shows the no-load and with-load (300 W) output voltages at V_{LV1} and V_{LV2}. In Fig. 10(a), the measured V_{LV1} (38.96 V) and V_{LV2} (39.02) were consistent with the simulation results shown in Fig. 7(a). Fig. 10(b) shows the experimental results when a 5-Ω resistive load was connected at the secondary-side LV node (LV2). At this condition, V_{LV1} and V_{LV2} reduced to 38.81 and 37.82 V, respectively. These voltages are also consistent with the simulation results shown in Fig. 7(b).

Fig. 11(a) and (b) shows the measured ac voltages across the primary-side windings of the transformer during no-load and full-load conditions. The secondary-side voltage of the transformer is shown and compared with the primary-side
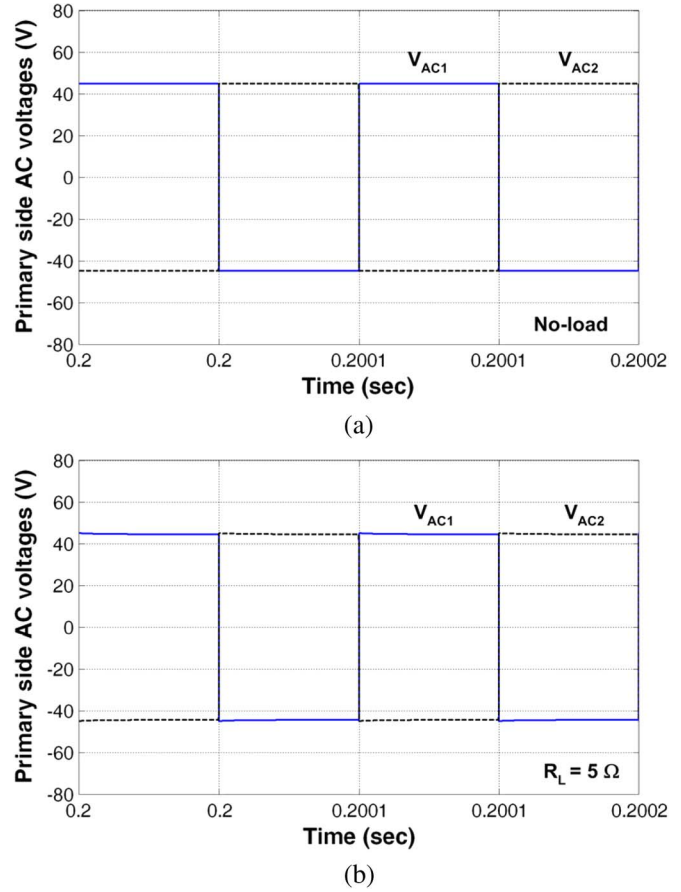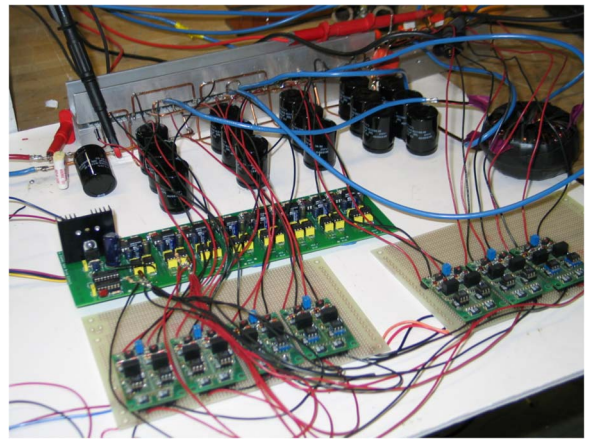

Fig. 9.   Four-hundred-watt prototype of the isolated MMCCC based on the schematic shown in Fig. 4.

voltage in Fig. 12(a) and (b). Thus, Figs. 11 and 12 show that all three windings of the transformer have the same turn ratio, and the dc voltage drop across the windings is minimum. The voltage variation between no load and full load is very small, and this is also shown in Fig. 10 (after rectification). From the experimental waveforms, it can be observed that the average value of primary-side voltages was zero ($average\ of\ V_{\mathrm{AC1}} + average\ of\ V_{\mathrm{AC2}}$). This is also true for the secondary side.
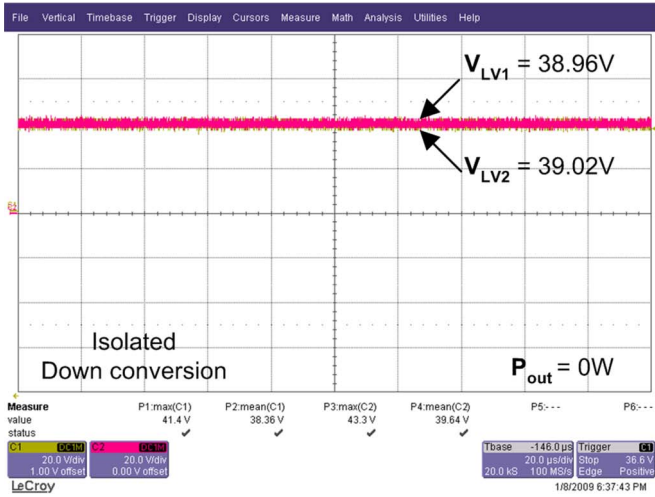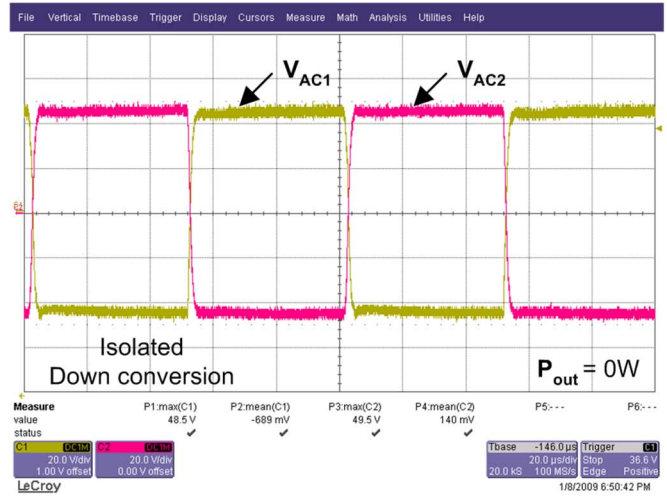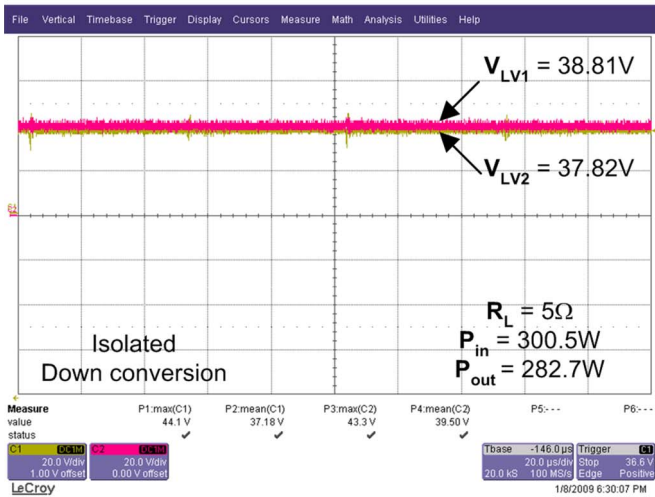
Fig. 10. Experimental results of the isolated MMCCC in the down-conversion (buck) mode. (a) LV side voltages at no-load condition. (b) LV side voltages at loade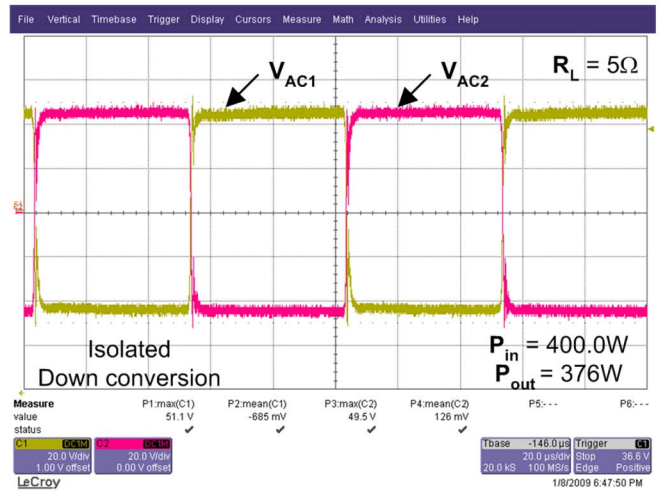d condition. V_{LV1} is the nonisolated LV side voltage; V_{LV2} is the isolated LV side voltage. In both cases, V_{HV1} was 155.96 V. Voltages are scaled at 20 V/div.

Fig. 11. Experimental results of the primary-side ac outputs of the MMCCC. (a) At zero load. (b) At 376-W loading condition. V_{HV1} was 179.75 V in both cases. Voltages are scaled at 20 V/div.

The HV and LV side characteristics of the nonisolated MMCCC are explained in Fig. 13. Fig. 13(a) shows the converter's input and output voltages in down-conversion (buck) mode. With a 5-Ω load connected at the LV side, the converter's output was 47.07 V with 190.98-V excitation at the HV side. The CR was 4.06 in this mode. When a 75-Ω load was connected at the HV side and a 42.9-V source was connected at the LV side, the HV side load voltage was 169.5 V, and this is shown in Fig. 13(b). The CR in this up-conversion (boost) mode was 3.95.

The efficiency characterization of the 400-W MMCCC prototype was performed in isolated and nonisolated modes. Fig. 14(a) shows the efficiency of the nonisolated MMCCC at various loading conditions. The efficiency of the converter was higher than 97.5% at full load for both up- and down-conversion modes. The efficiency profiling was also done in isolated mode for both up- and down-conversion operations, and this is shown in Fig. 14(b). The efficiency in the up-conversion mode was

higher than in the down-conversion mode, and this phenomenon was observed in previous versions of the MMCCC [17]. In the up-conversion mode, current flows through higher number of MOSFETs than diodes, and the conduction loss is smaller than it is in the down-conversion mode. The efficiency was higher than 95% in the up-conversion and just over 94% in the down-conversion mode for most of the operating range. The hardware detail of the prototype is shown in Table I.

The configuration shown in Fig. 2 was also constructed and experimentally tested. A six-level MMCCC and a four-level MMCCC were used to provide the bidirectional power transfer mechanism between the converter modules. A high-frequency ferrite core transformer made with 18 turns on the six-level MMCCC side and 19 turns on the four-level MMCCC side was used. An 84-V source was connected at V_{HV1}, and a 5-Ω resistive load was connected at V_{LV2}. Thus, the entire system was tested in no-load and partial load conditions. The circuit's switching frequency was 10 kHz.
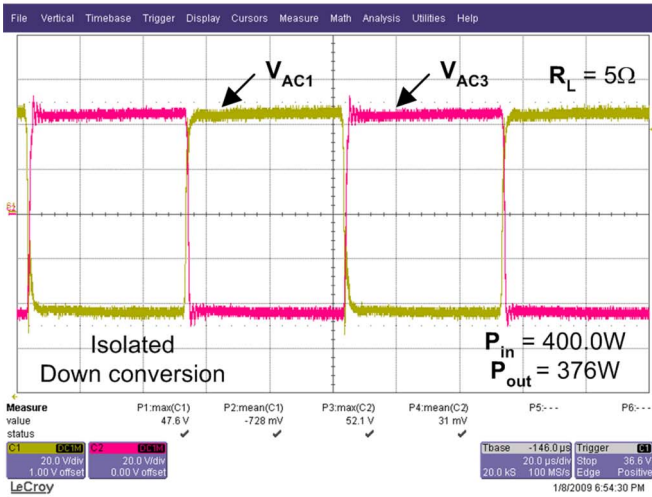
The circuit shown in Fig. 2 was tested by measuring the generated ac voltage at the secondary side of the transformer
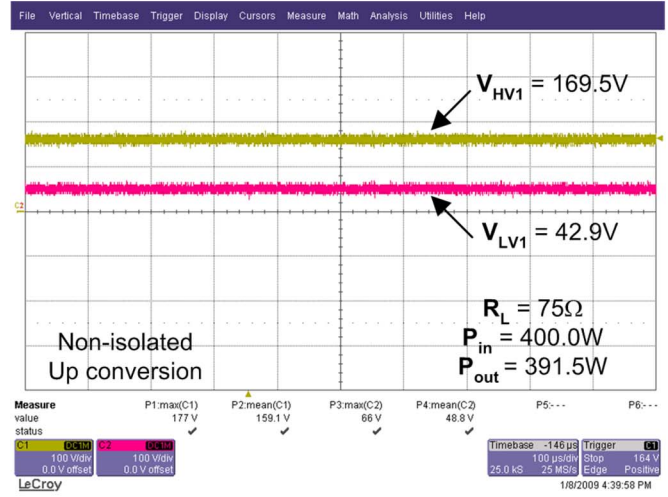
(a)
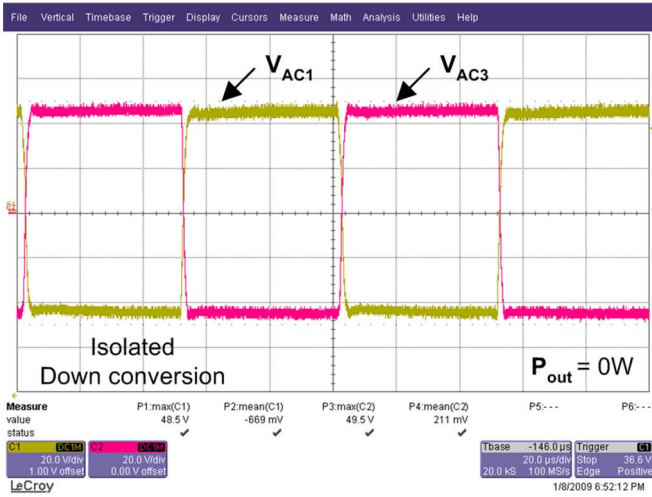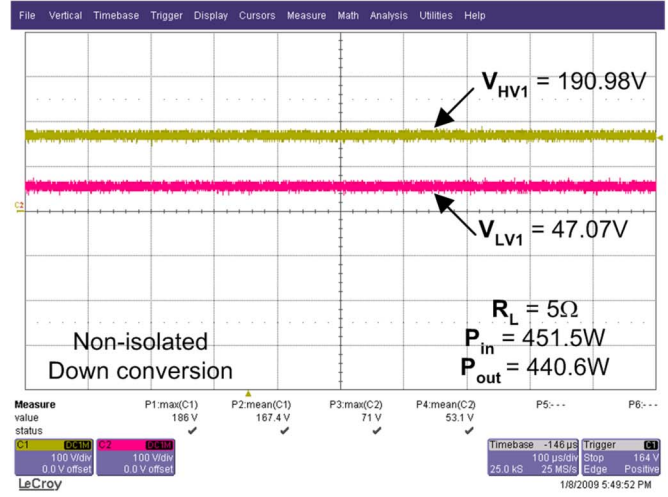
(b)

Fig. 12. Experimental results of the primary- and secondary-side ac outputs of the MMCCC. (a) At zero load. (b) At 376-W loading condition. $V_{\mathrm{HV1}} = 179.75$ V, and voltages are scaled at 20 V/div.

(a)

(b)

Fig. 13. Experimental results of the MMCCC in the nonisolated mode. (a) LV and HV side voltages in the down-conversion mode (buck mode). (b) LV and HV side voltages in the up-conversion mode (boost mode). Voltages are scaled at 100 V/div.

labeled as V_{ac2} in Fig. 2. Fig. 15(a) shows the voltage V_{ac2} at no-load condition, and the voltage amplitude was 13.8 V. When a 5-Ω load was connected at the V_{LV2} node, it drew some current and initiated the discharging operation across the capacitors in the four-level MMCCC circuit. The voltage V_{ac2} during this time is shown in Fig. 15(b). The voltages across the transformer had a small negative slope that indicates the decaying voltage across the clamp capacitors inside the MMCCC, and the magnitude of the slope depends on the load current, switching frequency, and the capacitance value in each module. The analytical verification of a four-level MMCCC thus further extends the origin of this voltage slope and has been investigated in Section VII.

VII. ANALYTICAL VERIFICATION

The start-up dynamic modeling and steady state analysis of a four-level MMCCC have been presented in [28], and capacitor voltages at various time instants can be found from

that analysis. The ac voltage swing produced at the MM-CCC is actually the potential difference across two adjacent capacitors' negative terminals, and this can be observed in Fig. 2. The equivalent circuits of a four-level MMCCC circuit in its subintervals are shown in Fig. 6 for analysis purposes. Fig. 6(a) shows the equivalent circuit during subinterval 1, and Fig. 6(b) shows that for the second subinterval. In the first subinterval, the negative terminal of C_2 is clamped to V_{C1} and that of C_3 is connected to ground. Thus, the voltage produced between V_{C3} and V_{C2} terminals is $-V_{C1}$. In the same way, this voltage is V_{C1} during the second subinterval, and the circuit orientation is shown in Fig. 6(b). Thus, the generated ac voltage between two adjacent nodes is $\pm V_{C1}$. Now, if the time varying voltage expression of V_{C1} can be found, the ac voltage swing of the MMCCC can be modeled for various loading conditions.

When loads are connected to the circuit, the capacitor voltages will depend on the load current and the time duration of the switching states. Using the analysis presented in [28], capacitor
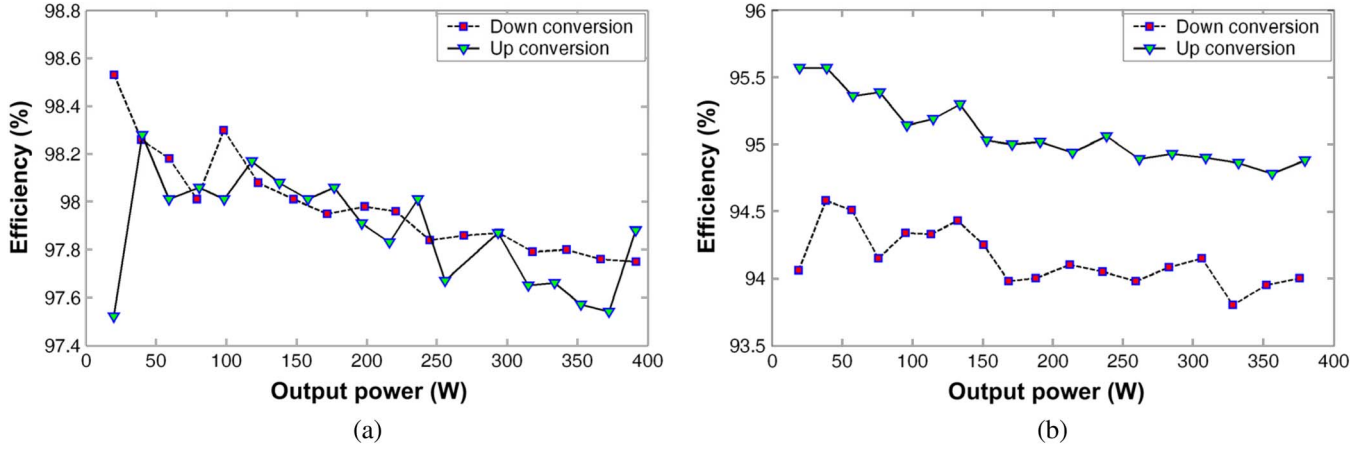
Fig. 14. Efficiency profiling of the MMCCC at nonisolated and isolated configurations. (a) Nonisolated configuration. (b) Isolated MMCCC.

TABLE I
EXPERIMENTAL SETUP FOR THE ISOLATED MMCCC

Parameter	Value
Transformer core type	Toroidal ferrite with $\mu = 10000$
No. of turns in each winding	20
MOSFET R_{DS}	0.017 Ω
$C_1 = C_2 = C_3 = C_4$	4500 μF
C_L	1500 μF
Switching frequency	10 kHz
Oscilloscope used	Lecroy Wavrunner 6030
Power supply used	TCR 10 kW Power Supply
Multimeter used	Fluke 87
Power analyzer used	Yokogawa WT230

voltages deduced for different time instants in a full operating cycle can be obtained. According to [28]

$$V_{C1}(t_1) = 0.25E + \delta_1 \quad (1)$$
$$V_{C1}(t_2) = 0.25E + \delta_1 - 0.2\Delta \quad (2)$$
$$V_{C1}(t_3) = V_{C2}(t_3) = 0.25E + 0.2\delta_2 + 0.02\Delta \quad (3)$$
$$V_{C1}(t_4) = 0.25E + 0.2\delta_2 - 0.18\Delta \quad (4)$$

where $\Delta = IL \bullet T/C$, I_L is the load current, T is the period of the switching frequency, C is the capacitor connected inside every module ($C_1 = C_2 = \cdots = C$), and $E = V_{HV2}$.

Now

$$\delta_1 = \frac{\Delta}{80} \qquad \delta_2 = -\frac{3\Delta}{80}. \quad (5)$$

Using (1) and (5)

$$V_{C1}(t_1) = \left(0.25E + \frac{\Delta}{80}\right). \quad (6)$$

Using (2) and (5)

$$V_{C1}(t_2) = 0.25E + \frac{\Delta}{80} - 0.2\Delta = \left(0.25E - \frac{3\Delta}{16}\right). \quad (7)$$

Using (3) and (5)

$$V_{C1}(t_3) = V_{C2}(t_3) = 0.25E + 0.2 \bullet \frac{3\Delta}{16} + 0.02\Delta$$
$$= \left(0.25E + \frac{\Delta}{80}\right). \quad (8)$$

Using (4) and (5)

$$V_{C1}(t_4) = 0.25E + 0.2 \bullet \frac{3\Delta}{16} - 0.18\Delta = \left(0.25E - \frac{3\Delta}{16}\right). \quad (9)$$

The time instants (t_1 to t_4) used in this calculation are synchronized with the timing diagram shown in Fig. 5, and the analytically computed values of V_{ac2} or ($V_{2b} - V_{3b}$) for a four-level configuration at different time instants are shown in Fig. 16 using (6)–(9). During the first subinterval, $V_{ac2} = -V_{C1}$, and the ac voltage is equal to V_{C1} during the second subinterval. Both the simulation and experimental results of the ac outputs of the converter show that the average voltage across any winding of the transformer is zero to confirm the volt–second balance in both subintervals of the operation. This is also observed from the voltages derived in the analytical computation.

VIII. OTHER NONISOLATED VERSIONS OF MMCCC

Future hybrid electric and plug-in hybrid vehicles may have many voltage buses with voltages ranging from 12 V to several hundred volts. The various topological configurations of internal combustion engine or fuel-cell-driven hybrid vehicles have been addressed in literatures [3]. When the 42-V loads need power from an HV source such as future 500–600-V bus, a high-efficiency converter topology with very high CR is required. Many favorable topologies could be adopted, and a special form of the MMCCC can be used, which can achieve very high CR from limited number of components. In addition, this modified MMCCC can also conserve the high-efficiency operation of the original MMCCC and retains the modular structure.

The original MMCCC has a nonisolated structure and requires $(3N - 2)$ transistors for a CR of N. For this reason, a great number of transistors are needed when the CR becomes high, and the circuit requires a larger form factor. This phenomenon is also observed in many other switched-capacitor circuits [29]–[31]. A universal module for the MMCCC was proposed in [32], where each module can generate a CR of two, and can work as an independent dc–dc converter. As a result, the heart of the universal MMCCC circuit is a four-transistor

(a)   (b)
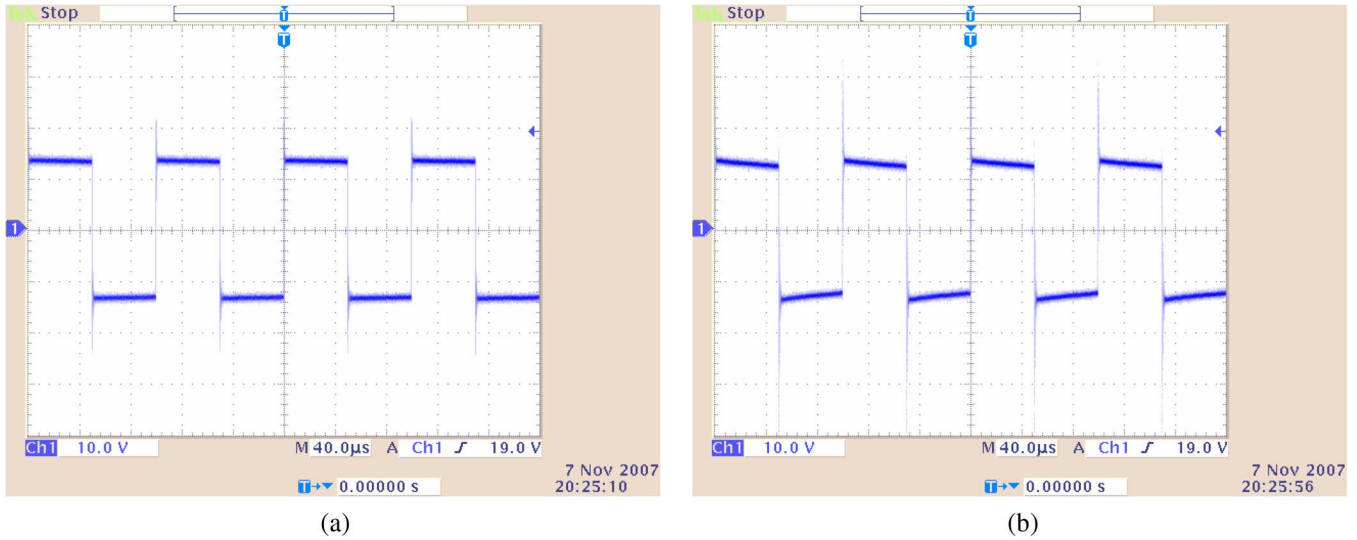
Fig. 15.   Experimental results of the isolated MMCCC built using the structure in Fig. 2. (a) Secondary-side voltage at no load. (b) Secondary-side voltage at loaded condition. Voltages are scaled at 10 V/div.
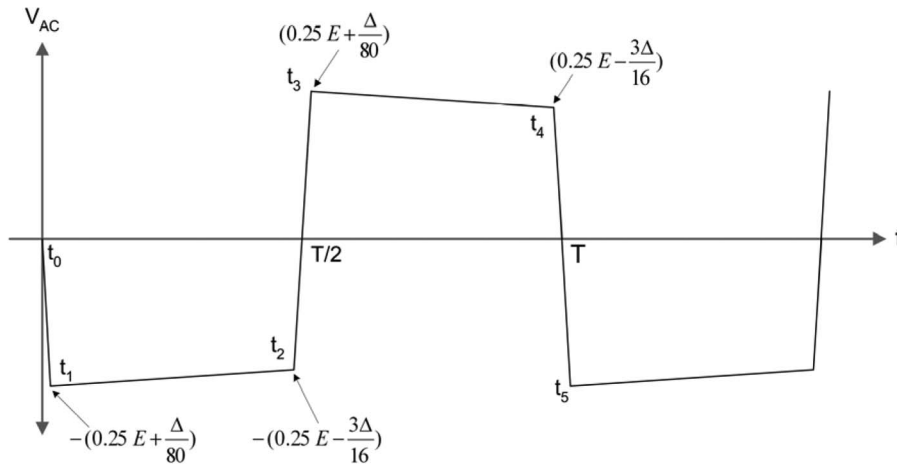

Fig. 16.   Analytical values derived for the ac voltage (V_{ac2}) generated across the transformer winding shown in Fig. 2.
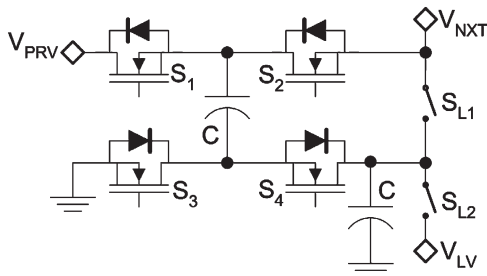

Fig. 17.   Four-transistor modular cell of the universal MMCCC.

two-capacitor cell shown in Fig. 17, which can bring many desirable features to the overall design of the MMCCC, and this is slightly different from the unit cell of the original MMCCC. In each cell, four transistors are grouped into two bootstrap pairs. Therefore, transistors S_1 and S_2 are driven by one bootstrap driver and S_3 and S_4 by another driver. Thus, the gate drive circuit remains almost the same in spite of having one more transistor in the cell. In the original MMCCC cell, there was only one capacitor [17]; however, two capacitors are

used in the new cell structure. Multiple cells are connected in a cascade pattern to form the converter, and a universal converter having three modules is shown in Fig. 18.

Inside each cell, there are two additional selector switches S_{L1} and S_{L2}, and these switches can be used to vary the CR of the overall circuit within a wide range. These switches are optional and can be avoided if the converter is operated in one fixed mode. On the other hand, the converter can be interchangeably operated in two different modes using the selector switches. These switches could be transistors or even electromechanical switches, depending on the application of the converter. The detailed operating principle of the converter is described in Section IX.

IX. UNIVERSAL MMCCC: CIRCUIT OPERATION

There are two operating modes of the universal MMCCC circuit. By selecting the proper states of S_{L1} and S_{L2}, any module can be configured interchangeably between modes. The operations of these two switches are complementary to each other.
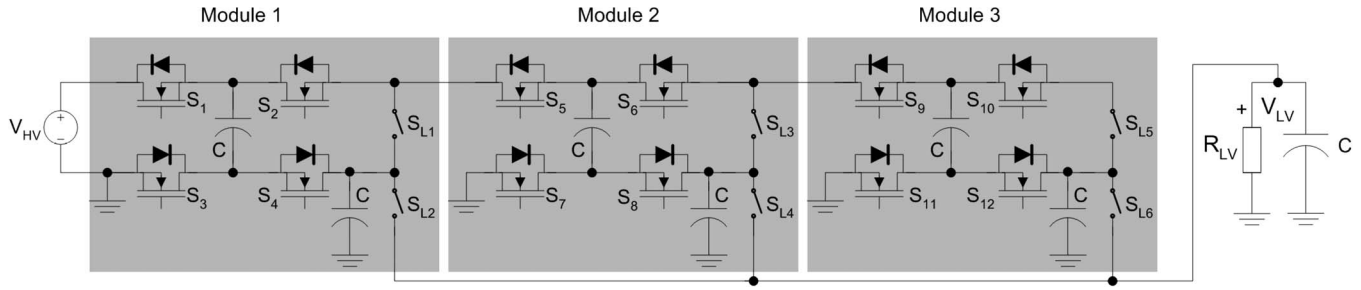
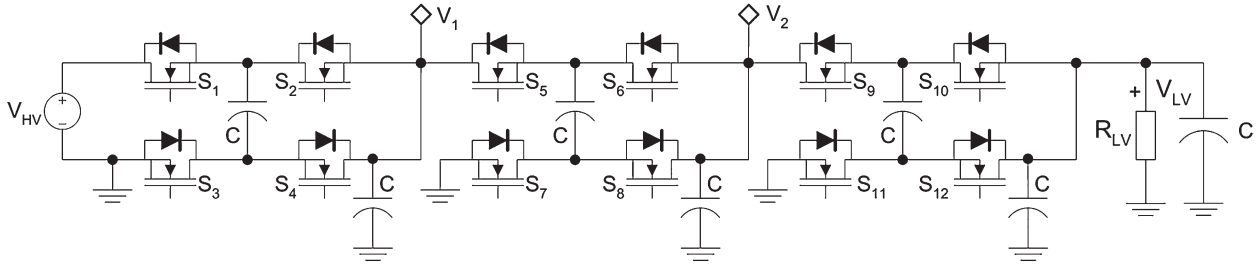Fig. 18.   Schematic of the universal MMCCC with three modules.

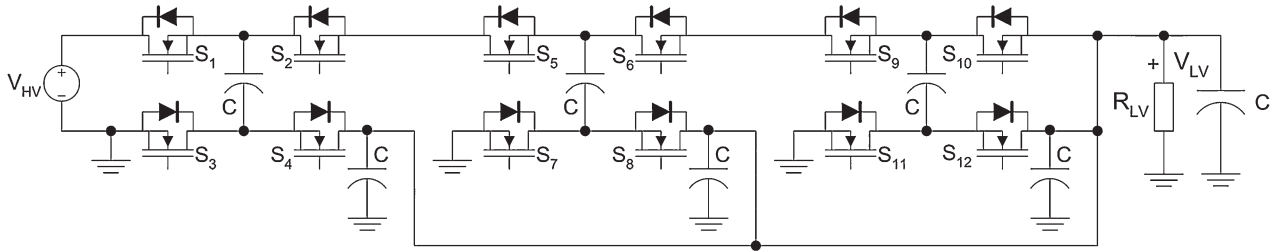Fig. 19.   Schematic of the universal MMCCC in the multiplier mode.

Fig. 20.   Schematic of the MMCCC in the normal mode.

A. Mode 1: Multiplier Mode

Inside each module, when S_{L1} is closed and S_{L2} is open, the module ends up working as a separate dc–dc converter with a CR equal to two. This mode can be defined as the multiplier mode. Thus, if S_{L1}, S_{L3}, S_{L5}, and S_{L6} are closed and S_{L2} and S_{L4} are open in Fig. 18, the CR of the circuit becomes $2 \times 2 \times 2 = 8$, and the operational diagram of the circuit is shown in Fig. 19.

B. Mode 2: Normal Mode

When S_{L1} is open and S_{L2} is closed inside each module, it works as a regular MMCCC module. When these modules are connected in a cascaded pattern, each module contributes a value of one toward the overall CR of the circuit. Thus, when S_{L1} and S_{L3} are open and S_{L2}, S_{L4}, S_{L5}, and S_{L6} are closed, the circuit works as a regular MMCCC circuit with a CR of four. The operational diagram of the corresponding circuit is shown in Fig. 20. This mode of operation of each module can be defined as the regular or normal mode.

Module 3 or the last module from the left is different from the other two modules, because in this module, both the selector switches S_{L5} and S_{L6} are permanently closed for the correct operation of the converter. Thus, module 3 always works in

the multiplier mode. The detailed operating principle of the MMCCC can be found in [17].

The circuit could be manipulated in many other ways to achieve CRs other than four and eight. When module 1 works in the multiplier mode and module 2 works in the regular mode inside a four-level converter with three modules, the cascade combination of modules 1 and 2 creates an MMCCC circuit with a CR of three. Moreover, module 3 always works in multiplier mode. Thus, when combined with module 3, the overall CR of the circuit becomes $3 \times 2 = 6$. When more modules are connected in cascade, more variations in the CR of the circuit can be achieved. In addition, when one of the three modules works in the multiplier mode and the other modules are bypassed [18], the circuit achieves the minimum CR of two. Thus, the overall CR of the circuit with three modules as shown in Fig. 18 can be two, three, four, six, or eight. Table II summarizes the possible CRs of a three-module converter by assigning different modes for the modules.

X. ACHIEVING LIMITED ISOLATION IN THE CIRCUIT

One of the key features of the new universal MMCCC circuit is the limited form of galvanic isolation in the circuit. The input and output of a capacitor-clamped circuit are not usually

TABLE II
CRs OF THE UNIVERSAL MMCCC FOR DIFFERENT OPERATING MODES OF
THE MODULES. B = BYPASS, M = MULTIPLIER, AND R = REGULAR

CR	Module 1	Module 2	Module 3
2	M	B	B
2	B	M	B
2	B	B	M
3	R	R	B
4	R	R	M
4	M	M	B
6	M	R	M
8	M	M	M

isolated, and there exists a current path between the HV and LV sides of the converter. This phenomenon is observed in FCMDC, MMCCC, series–parallel converter, and many other capacitor-clamped converters [33]. When the universal MM-CCC is operated in multiplier mode, it can be operated in such a way that the LV side can remain isolated from the HV side.

Like the original MMCCC circuit, the universal version also has two states of operation: states 1 and 2. In Fig. 21, S_1, S_4, S_6, S_7, S_9, and S_{12} can be operated in state 1, and the remaining six transistors are switched in state 2. However, there is a redundant switching scheme present in the operation of the circuit. In this scheme S_1, S_4, S_5, S_8, S_9, and S_{12} are operated in state 1, and the other transistors are operated in state 2. These schemes are shown in Table III.

The universal MMCCC circuit performs in the same way using any of these two schemes mentioned in the previous section. However, when operating in scheme 1, a limited form of galvanic isolation can be achieved between the HV and LV sides. Fig. 21(a) shows the schematic of a converter with a CR that is equal to eight, and this converter uses switching scheme 1. Fig. 21(b) shows the equivalent charge-flow diagram in state 1, and Fig. 21(c) shows the charge-flow diagram in state 2. Using this scheme, the LV side becomes isolated from the HV side during both states. In state 1, the HV source is coupled to module 1, and the LV side is coupled with module 2 through module 3. In state 2, the HV side is coupled with module 2 through module 1, and the LV side is coupled with module 3 only. The operating voltage in module 2 is 2 $V_{\rm LV}$ and 1 $V_{\rm LV}$ in module 3. Thus, in worst case, the LV side load experiences a current path through module 2, which is only 2 $V_{\rm LV}$. In contrast, the LV side load is powered by a current path that is connected to $V_{\rm HV}$ in the original MMCCC, FCMDC, or in a buck converter. Because the LV side shares the same ground with the HV side in the universal MMCCC, this isolation is considered to be limited and not as superior as magnetic isolation.

XI. COMPACTNESS FACTOR

The other attractive feature of the universal MMCCC circuit is the lower component count for a certain CR compared to

many other capacitor-clamped circuits, particularly when the CR is high. In capacitor-clamped or charge pump circuits, the CR is usually a constant integer number [33], and it requires a certain number of transistors to generate that CR. Thus, there exists a ratio of the number of transistors to the CR of the converter, and this ratio indicates the level of compactness of the converter. The lower the ratio, the better is the compactness. In an FCMDC demonstrated in [6]–[8], this compactness factor (CF) is two. For the original MMCCC circuit presented in [17], this factor is $(3 - 2/N)$ to have features such as modular structure and fault bypass capability. For the series–parallel converter, the CF is the same as the MMCCC circuit [29].

The magneticless dual voltage dc–dc converter has a modular structure [30]. However, the CF is $(N + 1)$, which could be very high when the CR is high. In a switched-capacitor step-up dc–dc converter [31], the CF is 3.33. By contrast, the universal MMCCC achieves a CR-dependent CF, and it could be as low as one, depending on the CR of the converter. Thus, the new circuit could achieve many desirable features of the MMCCC topology having a smaller number of transistors. The circuit shown in Fig. 19 has three modules requiring 12 transistors, and the maximum achievable CR is eight. Thus, CF is 1.5, which is already smaller than the FCMDC circuit. For a five-level universal MMCCC with four modules, the maximum achievable CR is 16, and the required number of transistors becomes 16 also. Thus, the CF is only one here. For higher number of modules, this factor drops below one, and the circuit becomes very compact.

For a converter with N modules, the minimum achievable CR would be two. However, the maximum $CR = 2^N$. One module needs four transistors. Thus, the total number of transistors = 4 N.

Thus

$$CF = \frac{4N}{2^N} = N \bullet 2^{(2-N)}. \qquad (10)$$

For $N = 4$, the CF becomes exactly one. When more modules are used to achieve higher CR, the CF drops in an exponential manner, and this is shown in Fig. 22.

XII. COMPONENT UTILIZATION (CU)

The universal MMCCC circuit has higher CF compared to several switched-capacitor converters such as FCMDC. However, the original MMCCC performs the best from the CU perspective. CU is defined as a ratio of the power handling capability of the converter and the total voltampere (VA) rating of the installed transistors in the converter. Thus, $CU = P_{\rm conv}/\sum V_{\rm max} \bullet I_{\rm max}$, where $P_{\rm conv}$ is the converter's power handling capability. $V_{\rm max}$ and $I_{\rm max}$ are the maximum voltage and current stress experienced by an individual transistor inside the converter, and these two parameters are prime factors to decide the physical size and price of the transistor. A small CU is an indication of utilizing a small fraction of the installed capacity of the converter. Thus, it is always preferred to achieve a higher CU for any design.

The following calculation shows the comparative analysis of CU for four different topologies. These calculations are done
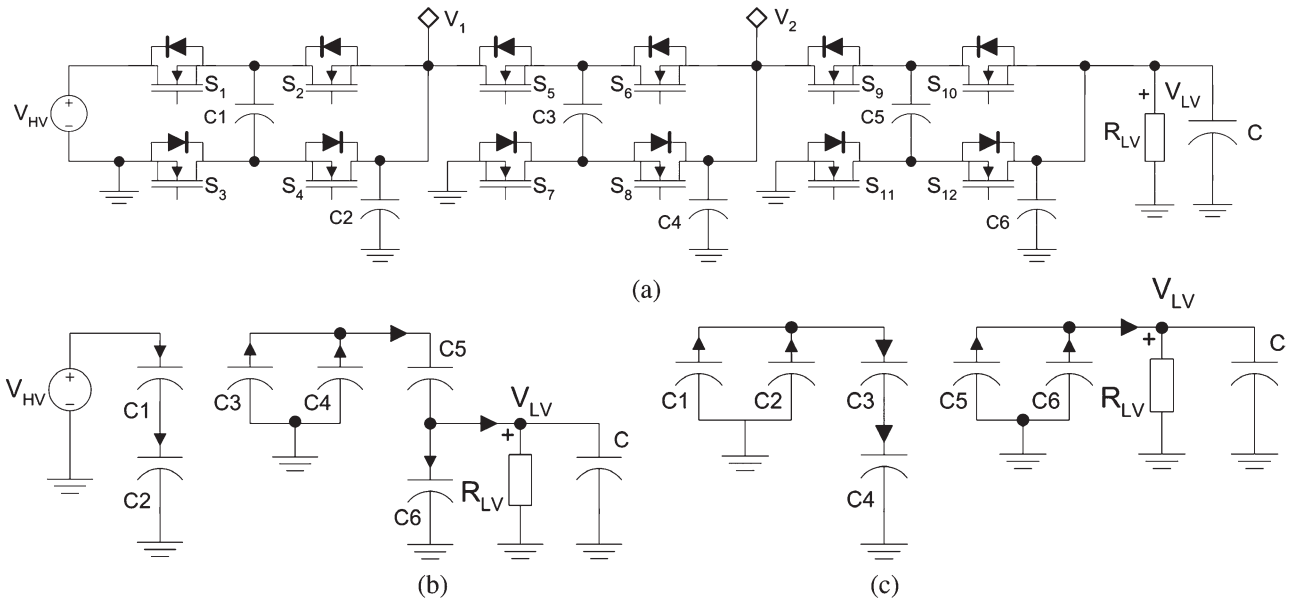
Fig. 21. (a) Universal MMCCC in the multiplier mode. (b) Equivalent circuit of the isolated MMCCC circuit in subinterval 1 (state 1). (c) Equivalent circuit in subinterval 2 (state 2). There is no closed current paths between the HV and LV sides during both operational states.

TABLE III
DIFFERENT SWITCHING SCHEMES OF THE UNIVERSAL MMCCC AND ACTIVE TRANSISTORS IN STATES 1 AND 2

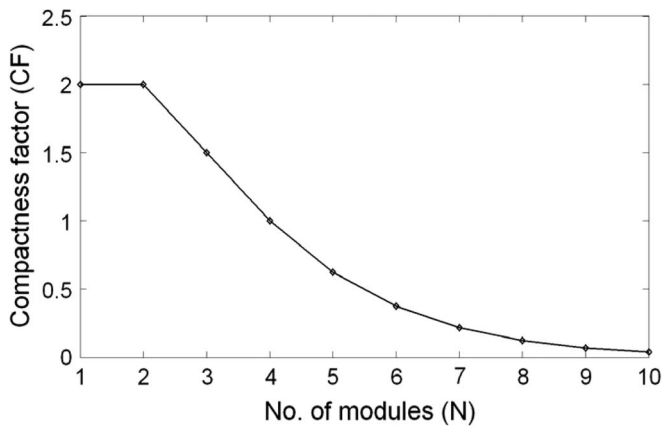|	Switching Scheme 1		Switching Scheme 2	
	State 1	State 2	State 1	State 2
	S_1	S_2	S_1	S_2
Active	S_4	S_3	S_4	S_3
Transistors	S_6	S_5	S_5	S_6
	S_7	S_8	S_8	S_7
	S_9	S_{10}	S_9	S_{10}
	S_{12}	S_{11}	S_{12}	S_{11}

Fig. 22. Graphical representation of the CF as a function of number of modules in the universal MMCCC.

based on a dc–dc converter, where V_{HV} is 40 V, V_{LV} is 5 V, and I_{LV} is 80 A; thus, the total output power is 400 W, considering the converter is operating in down-conversion (buck) mode.

A. Universal MMCCC

To obtain a CR equal to eight, the universal MMCCC needs three modules and 12 transistors, and this is shown in Fig. 19. Each transistor in module 1 experiences a maximum voltage stress of 0.5 V_{HV}, and a maximum current stress if 0.25 I_{LV}. In module 2, the maximum voltage stress is 0.25 V_{HV}, and the maximum current stress is 0.5 I_{LV}. In the last module, these stress figures are 0.125 V_{HV} and I_{LV}. Thus, the total installed capacity in VA is

$$(4 \bullet 20 \bullet 20) + (4 \bullet 10 \bullet 40) + (4 \bullet 5 \bullet 80) = 4800 \text{ VA.} \tag{11}$$

[With this calculation method, all of the modules cannot be identical (modular) if some have different current ratings or voltage ratings.]

B. Original MMCCC

For the original MMCCC, it requires seven modules and 22 transistors to obtain a CR of eight. There will be four parallel paths to deliver a load current of 80 A in this converter. According to the method shown in [18], the installed capacity in VA is

$$\left(5 \bullet 10 \bullet \frac{80}{4}\right) + \left(17 \bullet 5 \bullet \frac{80}{4}\right) = 2700 \text{ VA.} \tag{12}$$

C. FCMDC

For the FCMDC circuit, it takes 16 transistors to produce a CR equal to eight. According to [18], the installed VA of these 16 transistors is

$$(16 \bullet 5 \bullet 80) = 6400 \text{ VA.} \tag{13}$$

TABLE IV
CU AND CF OF VARIOUS DC–DC CONVERTERS

	MMCCC	Universal MMCCC	FCMDC	Buck	Series-parallel Converter	Inductorless dc-dc converter
CF	(3-2/N)	$N.2^{(2-N)}$	2	---	(3-2/N)	(N+1)
CU (for a 40V/5V, 400 W converter)	4/27	1/12	1/16	1/16	---	---

D. Buck Converter

For a single transistor classical buck converter, the transistor will experience a maximum voltage stress of 40 V and a maximum current stress of 160 A, considering the converter is operating in critical conduction mode. Thus, the installed VA rating would be

$$(1 \bullet 40 \bullet 160) = 6400 \text{ VA}. \tag{14}$$

This analysis shows that the original MMCCC has the best CU among these four topologies. Although the universal MMCCC does not have the best CU, it yields the best CF. Thus, there is a tradeoff in the design of the universal version that optimizes the CF by sacrificing some CU. The CF and CU of various dc–dc converters are summarized in Table IV.

XIII. UNIVERSAL MMCCC: SIMULATION RESULTS

To verify the concept of the universal MMCCC circuit, a four-level (three-module) universal MMCCC circuit was simulated in PSIM, and voltages at several nodes were observed. These results are summarized in Fig. 23. The converter was simulated in the down-conversion (buck) mode, and the universal feature of the converter was observed in two steps. In the first step, all the modules in the converter were configured to work in multiplier mode, and the overall CR was fixed at eight. The HV side voltage was 40 V, and a 5-Ω load was connected at the LV side. Some nonidealities such as MOSFET R_{DS} and capacitor ESR were considered while simulating the circuit. Based on the actual MOSFETs and capacitors used in the prototype, the R_{DS} that is equal to 0.052 Ω and an ESR of 100 mΩ were used in the simulation. In this mode, the output at the LV side is shown in Fig. 23(a), and the load voltage was 4.85 V. When the converter is simulated in a regular mode, the CR becomes four, and the corresponding output voltage is shown in Fig. 23(b). From the simulation, this voltage was found to be 9.9 V. In the last step, the converter was operated in the multiplier mode, and the voltages at V_{HV}, V_1, V_2 (shown in Fig. 19), and V_{LV} were observed simultaneously. This is shown in Fig. 23(c).

From Fig. 23(a), it can be seen that the concept of the new topology works, and the circuit can also work as a combination of three individual MMCCC circuits. In addition, Fig. 23(b) shows that this universal converter circuit can also work as a regular MMCCC circuit. Thus, the introduction of the new modular cell presents a unified approach that can create a link between the original MMCCC and the modified MMCCC operating in the multiplier mode. Finally, Fig. 23(c) shows that
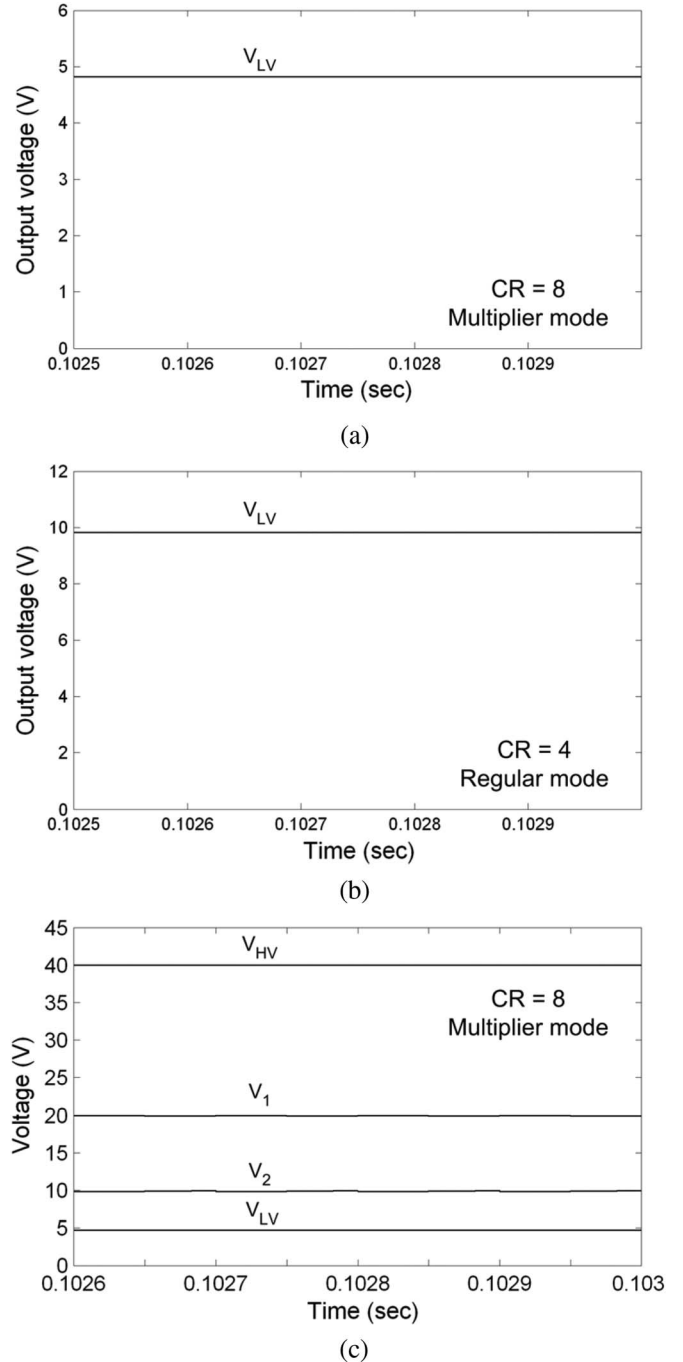

Fig. 23. Simulation results of the universal MMCCC. (a) LV side voltage in the multiplier mode. (b) LV side voltage in the regular mode. (c) Various node voltages in the multiplier mode.
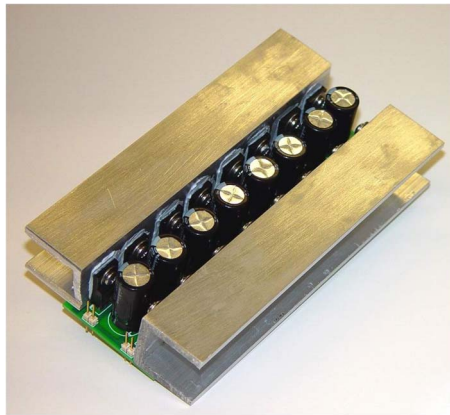
Fig. 24. Proof of concept prototype of the universal MMCCC.

the overall CR of the converter is the product of CRs of three individual converters. This is why V_1 is approximately two times V_2, and V_2 is about two times V_{LV}.
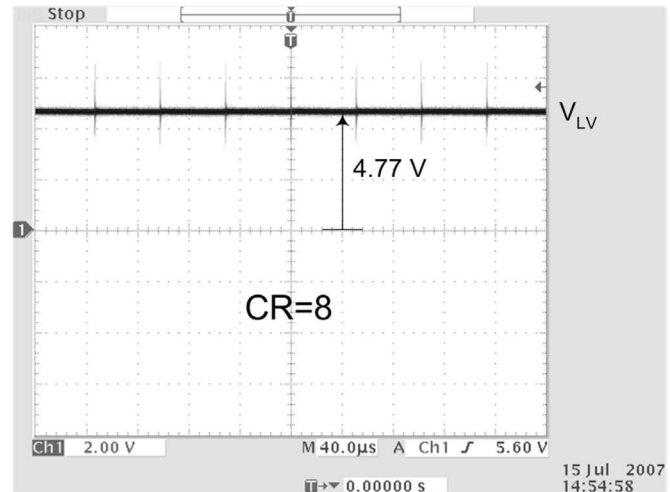
XIV. UNIVERSAL MMCCC: EXPERIMENTAL RESULTS

For a complete verification of the concept, a five-level (four-module) universal converter was fabricated and tested in both modes. Fig. 24 shows the photograph of the converter. By using appropriate gate signals, three out of these four modules were used to generate the experimental results. Four IRFI540N MOSFETs and two 1000-μF general purpose electrolytic capacitors were used to form one module. Two bootstrap gate drive circuits (IR2110) were used to drive four MOSFETs inside each module.

In the first step, the converter was configured in the multiplier mode, and in this mode, the CR was eight. For an input voltage of 40 V, the theoretical output voltage should be 5 V at no-load condition. With a 5-Ω load at the output, the LV side voltage was recorded and shown in Fig. 25(a), and the measured voltage was 4.77 V. By configuring the converter in a regular mode, the CR became four, and the corresponding output voltage is shown in Fig. 25(b). This time, the voltage found at the LV side was 9.69 V.

In the third step, the converter was operated in the multiplier mode, and the voltages V_1, V_2, and V_{LV} in Fig. 19 were recorded; they are shown in Fig. 25(c). From this experiment, it can be shown that the overall CR of the circuit is a product of the CRs of individual MMCCC circuits. V_1 is the output of module 1, and this is approximately half of V_{HV}. Again, V_1 works as the input of module 2, and V_2 is the output of module 2. Thus, V_2 is close to one half of V_1. Finally, V_2 works as the input to module 3, and it is about two times of V_{LV}. Therefore, the use of these three modules in the circuit can produce various outputs such as $V_{HV}/2$, $V_{HV}/4$, and $V_{HV}/8$ without changing the mode. Also from [32], the universal MMCCC circuit can generate other dc voltage levels by changing the mode into the regular configuration.

XV. CONCLUSION AND FUTURE WORK

Several new configurations to obtain isolated bidirectional dc outputs from a capacitor-clamped dc–dc converter (MMCCC)

(a)
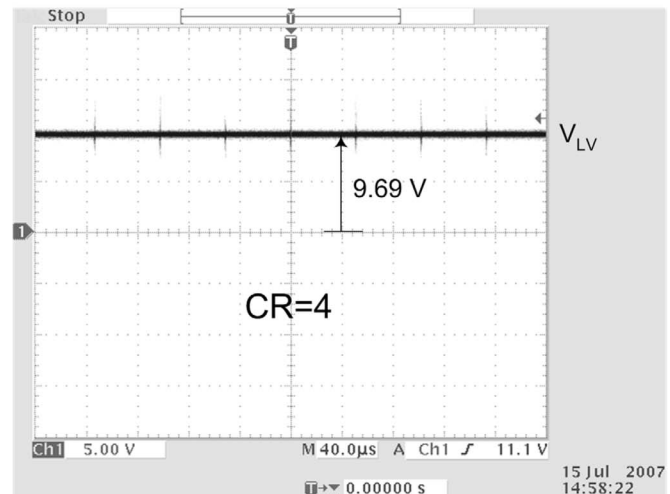
(b)
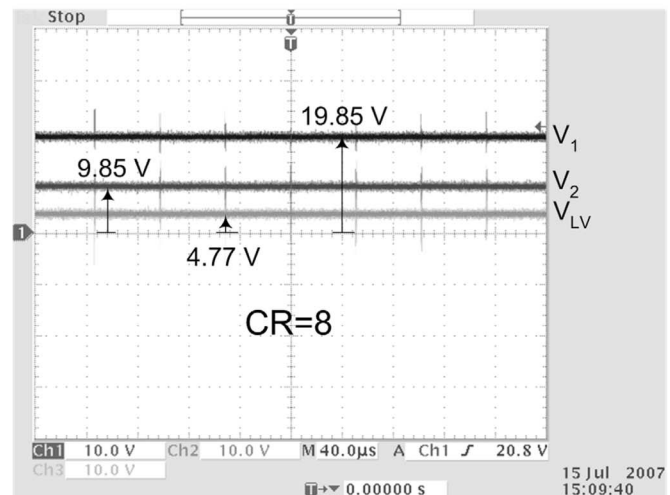
(c)

Fig. 25. Experimental results of the universal MMCCC. (a) LV side voltage in the multiplier mode (2 V/div). (b) LV side voltage in the regular mode (5 V/div). (c) Various node voltages in the multiplier mode (10 V/div).

have been proposed, and the concept has been verified using simulation, analytical, and experimental results. The experimental results show that isolated dc voltage outputs can be

generated from one part of the circuit while a voltage source is connected to the other part, and these two parts are interlinked through a high-frequency transformer. Using a transformer with a turn ratio other than 1 : 1, it is possible to generate many other voltage levels. This paper has shown four possible configurations to generate isolated dc voltages. However, it is possible to deduce many other configurations using single- or multi-winding transformers with bridge or center-tap configurations. Future hybrid or plug-in hybrid vehicles could be a great application of the isolated MMCCC, where it could be integrated with multiple sources such as battery, fuel cell, solar cell, ultracapacitors, and various loads as well. In addition, a universal form of the original MMCCC has also been presented in this paper, which can change its operating mode and achieve very large CR using a minimum number of components, thereby achieving a high CF. In addition to the isolated version, the universal version could also find applications in the electrical system of the future hybrid, plug-in hybrid, and fuel-cell vehicles.

REFERENCES

[1] A. Emadi, Y. J. Lee, and K. Rajashekhara, "Power electronics and motor drives in electric, hybrid electric and plug-in hybrid electric vehicles," *IEEE Trans. Ind. Electron.*, vol. 55, no. 6, pp. 2237–2245, Jun. 2008.

[2] L. Tang and G. J. Su, "An interleaved, reduced component count, multi-voltage bus DC/DC converter for fuel cell powered electric vehicle applications," in *Conf. Rec. IEEE IAS Annu. Meeting*, 2007, pp. 616–621.

[3] A. Emadi, S. Williamson, and A. Khaligh, "Power electronics intensive solutions for advanced electric, hybrid electric, and fuel cell vehicular power systems," *IEEE Trans. Power Electron.*, vol. 21, no. 3, pp. 567–577, May 2006.

[4] M. H. Todorovic, L. Palma, and P. N. Enjeti, "Design of a wide input range DC_DC converter with a robust power control scheme suitable for fuel cell power conversion," *IEEE Trans. Ind. Electron.*, vol. 53, no. 4, pp. 1094–1104, Aug. 2006.

[5] H.-J. Chiu and L.-W. Lin, "A bi-directional DC–DC converter for electric vehicle driving system," *IEEE Trans. Power Electron.*, vol. 21, no. 4, pp. 950–958, Jul. 2006.

[6] M. Shen, F. Peng, and L. Tolbert, "Multilevel DC–DC power conversion system with multiple DC sources," *IEEE Trans. Power Electron.*, vol. 23, no. 1, pp. 420–426, Jan. 2008.

[7] F. Zhang, L. Du, F. Z. Peng, and Z. Qian, "A new design method for high-power high-efficiency switched-capacitor DC–DC converters," *IEEE Trans. Power Electron.*, vol. 23, no. 2, pp. 832–840, Mar. 2008.

[8] F. Z. Peng, F. Zhang, and Z. Qian, "A novel compact DC–DC converter for 42 V systems," in *IEEE PESC*, Jun. 2003, pp. 33–38.

[9] H. Li, F. Z. Peng, and J. S. Lawler, "A natural ZVS medium-power bidirectional DC–DC converter with minimum number of components," *IEEE Trans. Ind. Appl.*, vol. 39, no. 2, pp. 525–535, Mar./Apr. 2003.

[10] E. Hiraki, K. Yamamoto, T. Tanaka, and T. Mishima, "An isolated bi-directional DC–DC soft switching converter for super capacitor based energy storage systems," in *Proc. IEEE PESC*, 2007, pp. 390–395.

[11] Z. Jiang and R. A. Dougal, "A compact digitally controlled fuel cell/battery hybrid power source," *IEEE Trans. Ind. Electron.*, vol. 55, no. 6, pp. 2237–2245, Jun. 2008.

[12] G.-J. Su and F. Z. Peng, "A low cost, triple-voltage bus DC–DC converter for automotive applications," in *Proc. IEEE APEC*, Mar. 2005, vol. 2, pp. 1015–1021.

[13] C.-W. Roh, S.-H. Han, S.-S. Hong, S.-C. Sakong, and M.-J. Youn, "Dual-coupled inductor-fed DC/DC converter for battery drive applications," *IEEE Trans. Ind. Electron.*, vol. 51, no. 3, pp. 577–584, Jun. 2004.

[14] H. Mao, L. Yao, C. Wang, and I. Batarseh, "Analysis of inductor current sharing in nonisolated and isolated multiphase DC–DC converters," *IEEE Trans. Ind. Electron.*, vol. 54, no. 6, pp. 3379–3388, Dec. 2007.

[15] R.-J. Wai, C.-Y. Lin, R.-Y. Duan, and Y.-R. Chang, "High efficiency DC–DC converter with high voltage gain and reduced switch stress," *IEEE Trans. Ind. Electron.*, vol. 54, no. 1, pp. 354–364, Feb. 2007.

[16] M. T. Zhang, M. M. Jovanovic', and F. C. Y. Lee, "Analysis and evaluation of interleaving techniques in forward converters," *IEEE Trans. Power Electron.*, vol. 13, no. 4, pp. 690–698, Jul. 1998.

[17] F. H. Khan and L. M. Tolbert, "A multilevel modular capacitor-clamped DC–DC converter," *IEEE Trans. Ind. Appl.*, vol. 43, no. 6, pp. 1628–1638, Nov. 2007.

[18] F. H. Khan and L. M. Tolbert, "A 5-kW multilevel DC–DC converter for future hybrid electric and fuel cell automotive applications," in *Conf. Rec. IEEE IAS Annu. Meeting*, 2007, pp. 628–635.

[19] L. Solero, A. Lidozzi, and J. A. Pomilio, "Design of multiple-input power converter for hybrid vehicles," *IEEE Trans. Power Electron.*, vol. 20, no. 5, pp. 1007–1016, Sep. 2005.

[20] H. Matsuo, W. Lin, F. Kurokawa, T. Shigemizu, and N. Watanabe, "Characteristics of the multiple-input DC–DC converter," *IEEE Trans. Ind. Electron.*, vol. 51, no. 3, pp. 625–631, Jun. 2004.

[21] K. P. Yalamanchili and M. Ferdowsi, "Review of multiple input DC–DC converters for electric and hybrid vehicles," in *Proc. IEEE VPPC*, 2005, pp. 160–163.

[22] Y.-M. Chen, Y.-C. Liu, and F.-Y. Wu, "Multiple-input DC/DC converter based on the multiwinding transformer for renewable energy applications," *IEEE Trans. Ind. Appl.*, vol. 38, no. 4, pp. 1096–1104, Jul./Aug. 2002.

[23] Y.-C. Liu and Y.-M. Chen, "A systematic approach to synthesizing multi-input DC/DC converters," in *Proc. IEEE PESC*, 2007, pp. 2626–2632.

[24] B. G. Dobbs and P. L. Chapman, "A multiple-input DC–DC converter topology," *IEEE Power Electron. Lett.*, vol. 1, no. 1, pp. 6–9, Mar. 2003.

[25] F. H. Khan and L. M. Tolbert, "Multiple load-source integration in a multilevel modular capacitor clamped DC–DC converter featuring fault tolerant capability," in *Proc. IEEE APEC*, Feb. 2007, pp. 361–367.

[26] F. H. Khan and L. M. Tolbert, "A 5 kW bi-directional multilevel modular DC–DC converter (MMCCC) featuring built in power management for fuel cell and hybrid electric automobiles," in *Proc. IEEE VPPC*, 2007, pp. 208–214.

[27] A. I. Pressman, *Switching Power Supply Design*. New York: McGraw-Hill, 1998, ch. 6.

[28] F. H. Khan, "Modular DC–DC converters," Ph.D. dissertation, Univ. Tennessee, Knoxville, TN, Apr. 2007.

[29] W. Harris and K. Ngo, "Power switched-capacitor DC–DC converter, analysis and design," *IEEE Trans. Aerosp. Electron. Syst.*, vol. 33, no. 2, pp. 386–395, Apr. 1997.

[30] F. Z. Peng, F. Zhang, and Z. Qian, "A magnetic-less DC–DC converter for dual voltage automotive system," *IEEE Trans. Ind. Appl.*, vol. 39, no. 2, pp. 511–518, Mar. 2003.

[31] O. Mak, Y. Wong, and A. Ioinovici, "Step-up DC power supply based on a switched-capacitor circuit," *IEEE Trans. Ind. Electron.*, vol. 42, no. 1, pp. 90–97, Feb. 1994.

[32] F. H. Khan and L. M. Tolbert, "Universal multilevel DC–DC converter with variable conversion ratio, high compactness factor and limited isolation feature," in *Proc. IEEE APEC*, Feb. 2008, pp. 17–23.

[33] M. D. Seeman and S. R. Sanders, "Analysis and optimization of switched-capacitor DC–DC converters," *IEEE Trans. Power Electron.*, vol. 23, no. 2, pp. 841–851, Mar. 2008.

Faisal H. Khan (S'01–M'07) received the B.S. degree in electrical engineering from Bangladesh University of Engineering and Technology, Dhaka, Bangladesh, in 1999, the M.S. degree in electrical engineering from Arizona State University, Tempe, in 2003, and the Ph.D. degree in power electronics from The University of Tennessee, Knoxville, in 2007.

He has been a Senior Project Engineer with the Electric Power Research Institute, Knoxville, TN, since April 2007. His research interests include dc–dc converters, hybrid electric and fuel-cell automobile power management, and power supply efficiency issues.

Dr. Khan received the 2007 First Prize Paper Award of the Industrial Power Converter Committee in the IEEE/Industry Applications Society Annual Meeting. He is a member of IEEE Power Electronics Society, Industry Application Society, and Industrial Electronics Society. He has served as a Reviewer and the Session Chair of IEEE transactions and conferences.

Leon M. Tolbert (S'89–M'91–SM'99) received the Bachelor's, M.S., and Ph.D. degrees in electrical engineering from the Georgia Institute of Technology, Atlanta, in 1989, 1991, and 1999 respectively.

He was with the Engineering Division, Oak Ridge National Laboratory, Knoxville, TN, in 1991. He was appointed as an Assistant Professor with the Department of Electrical and Computer Engineering, The University of Tennessee, Knoxville, in 1999. He is currently a Min Kao Professor with the Min Kao Department of Electrical Engineering and Computer Science, The University of Tennessee. He is also a Research Engineer with the Power Electronics and Electric Machinery Research Center, Oak Ridge National Laboratory.

Dr. Tolbert is a Registered Professional Engineer in the state of Tennessee. He is the recipient of an NSF CAREER Award in 2001, the 2001 IEEE Industry Applications Society Outstanding Young Member, and two prize paper awards from the IEEE Industry Applications Society Annual Meeting. From 2003 to 2006, he was the Chairman of the Education Activities Committee of the IEEE Power Electronics Society and an Associate Editor for the IEEE POWER ELECTRONICS LETTERS. He has been an Associate Editor of the IEEE TRANSACTIONS ON POWER ELECTRONICS since 2007.

William E. Webb (S'00–M'06) received the B.S. degrees in electrical engineering and in computer engineering from North Carolina State University, Raleigh, and the M.S. degree in electrical and computer engineering from the Georgia Institute of Technology, Atlanta.

He is a Project Engineer and a Scientist with the Electric Power Research Institute (EPRI), Knoxville, TN. Before joining EPRI, he was a Senior Electrical Engineer with CSC Advanced Marine Enterprises, Washington, DC, providing total ship acquisition support to several branches of the armed forces of the U.S., including the Navy, Marine Corps, Army, and Coast Guard. He was responsible for the overall design, specification, and integration of ships' electrical systems, many of which utilized electric propulsion. His current research activities focus on critical power.